RASĀYAN *J. Chem.*
Vol. 17 | No. 2 |642-656| April - June | 2024
ISSN: 0974-1496 | e-ISSN: 0976-0083 | CODEN: RJCABP
http://www.rasayanjournal.com
http://www.rasayanjournal.co.in

GREEN SYNTHESIS OF FE NANOPARTICLES FROM *Cissus quadrangularis* AND EVALUATING ITS PHOTOCATALYTIC EFFICACY OF METHYL ORANGE USING RESPONSE SURFACE METHODOLOGY

Hemapriya Janarthanam[1,✉], Reshma Girirajan[1], Rajalakshmi Balaji[1] and Vijayanand Selvaraj[2]

[1]PG and Research Department of Microbiology, DKM College for Women (Autonomous), Vellore-632 001

[2]Department of Biotechnology, Thiruvalluvar University, Serkkadu, Vellore-632 115

✉Corresponding Author: bentresearchgroup2018@gmail.com

ABSTRACT

In an era where environmental stewardship is paramount, the rampant release of azo dyes into our ecosystems by textile and related industries presents a pressing concern. Among these dyes, Methyl Orange (MO), a textile industry staple, emerges as a significant component of industrial waste, pervading various water sources and precipitating pollution. The imperative for its decomposition, particularly in the context of potable water, cannot be overstated. The pernicious cocktail of dye residues, bacterial contaminants, and antibiotic remnants has engendered a perilous milieu for both fauna and humanity alike, underscoring the urgent need for versatile agents capable of mitigating diverse pollutants. Enter nanotechnology, a transformative force empowering the genesis of precise and efficacious methodologies for wastewater treatment, irrespective of scale. In this pioneering endeavour, our aim is twofold: first, to synthesize iron (Fe) nanoparticles utilizing the stem aqueous extract of *Cissus quadrangularis*, and second, to meticulously characterize these biosynthesized Fe nanoparticles through a suite of analytical techniques including UV spectroscopy, XRD, FTIR, Zeta potential with DLS and SEM-EDAX examination. Moreover, we embark on a quest to unravel the potential of these biologically derived Fe particles in catalysing the photo-degradation of methyl orange under the aegis of UV radiation, coupled with an assessment of methyl orange biodegradation via UV-Vis spectroscopy analysis. Central to our methodology is the employment of an experimental design paradigm, underpinned by the venerable Response Surface Methodology (RSM), to forge a blueprint for optimizing the operational variables germane to the photocatalytic degradation of methyl orange utilizing Fe nanoparticles. Through this concerted effort, we aspire not merely to mitigate the deleterious impact of industrial effluents, but to usher forth a new epoch of sustainable and efficacious wastewater treatment methodologies.

Keywords: Environmental Stewardship, Azo Dyes, Textile Industry, Industrial Waste, Pollution, Iron Nanoparticles, Nanotechnology, Methyl Orange, Response Surface Methodology (RSM), Central Composite Design (CCD).

RASĀYAN *J. Chem.*, Vol. 17, No.2, 2024

INTRODUCTION

Azo dyes represent a ubiquitous presence in diverse industrial sectors, including printing, textiles, paper, cosmetics, and leather. The magnitude of their impact is staggering, with over 70% of wastewater generated by these industries containing substantial quantities of dye contaminants.[1] Textile manufacturers, in particular, contribute significantly to this environmental burden through the extensive use of various dyes in their production processes, resulting in the discharge of pollutants that are notorious for their non-biodegradable nature and high toxicity levels.[2] The repercussions of this contamination extend far beyond industrial premises, as the dye pollutants infiltrate water systems, ultimately jeopardizing the integrity of drinking water sources. Efforts to mitigate this looming environmental crisis have spurred considerable research endeavours spanning multiple disciplines, ranging from physicochemical and biochemical approaches to analytical methodologies.[3] However, the efficacy of traditional techniques is marred by their exorbitant costs and limited effectiveness, exacerbating concerns over the persistence and harmful effects of dye pollutants.[4] In this landscape of environmental urgency, heterogeneous Photocatalysis emerges as a promising avenue for pollutant remediation. Titanium dioxide (TiO_2), renowned for its exceptional degradation efficiency, has long been heralded as a frontrunner in this domain.[5] Yet, the burgeoning field of nanotechnology has ushered in a new era of possibilities, offering cost-effective alternatives for dye

http://doi.org/10.31788/RJC.2024.1728765

degradation. Recent studies have unveiled the potential of semiconductor nanocrystals to serve as potent photocatalysts, capitalizing on their unique band gap properties to harness solar energy for pollutant breakdown.[6] The advent of nanotechnology has revolutionized conventional approaches to nanoparticle synthesis, veering away from environmentally detrimental chemical processes towards more sustainable and eco-friendly methodologies.[7] Plant-mediated synthesis, in particular, has emerged as a beacon of promise, leveraging the inherent stability and rapid synthesis capabilities of plant components to produce well-functionalized fine particles. *Cissus quadrangularis* frequently called as "Veldt grape" or "Devil's backbone," is a perennial plant belonging to the grape family (Vitaceae). It is native to the Indian subcontinent, where it has been traditionally used in Ayurveda medicine for various medicinal purposes. The plant is characterized by its succulent, quadrangular (square-shaped) stems and fleshy leaves. In recent years, *Cissus quadrangularis* has gained attention in the space of nanotechnology and materials science for its potential in synthesizing metal nanoparticles, particularly iron (Fe) nanoparticles. The stem extract of *Cissus quadrangularis* has been identified as a promising bio-reducing agent for the synthesis of Fe nanoparticles through green synthesis methods. These methods offer eco-friendly alternatives to conventional chemical synthesis routes, minimizing the use of hazardous chemicals and reducing environmental impact. Several studies have demonstrated the efficacy of *Cissus quadrangularis* in facilitating the synthesis of Fe nanoparticles with desirable properties for various applications. For instance, research by Jeevanandam *et al.* (2020)[8] explored the use of *Cissus quadrangularis* stem extract for the eco-friendly synthesis of Fe particles and investigated their antimicrobial activity. The study found that the biosynthesized Fe nanoparticles exhibited significant antimicrobial properties against a range of pathogenic microorganisms, highlighting their potential in biomedical and environmental applications. Furthermore, investigations by Sharma *et al.* (2021)[9] focused on optimizing the synthesis parameters for the production of Fe nanoparticles using *Cissus quadrangularis extract.* Through systematic experimentation and characterization techniques such as UV-visible spectroscopy, FTIR, XRD, and TEM analysis, the study elucidated the influence of various factors based on the size, morphology, and stability of the biologically synthesized nanoparticles. These findings contribute to the understanding of the green synthesis process and pave the way for the development of Fe nanoparticles with tailored properties for specific applications, including wastewater treatment and catalysis. Overall, *Cissus quadrangularis* holds a promising sustainable and cost-effective precursor for the biogenesis of Fe nanoparticles through green synthesis methods. Further research in this area is warranted to explore the full potential of these nanoparticles and their applications in diverse fields, ranging from medicine to environmental remediation.[10] In alignment with this ethos of sustainability and innovation, the present study endeavours to harness the bio-reduction capabilities of *Cissus quadrangularis* stem aqueous extract for the facile synthesis of iron (Fe) nanoparticles. These biosynthesized nanoparticles are subjected to comprehensive characterization using a suite of analytical methods, including UV-Vis spectroscopy, FTIR, Zeta potential analysis, XRD, and SEM-EDAX. The focal point of our investigation lies in the application of these biologically derived Fe nanoparticles for the degradation of methyl orange, a prominent dye pollutant, under the influence of UV radiation. Additionally, the efficacy of this degradation process is evaluated through UV-Vis spectroscopy analysis, elucidating the intricate mechanisms underlying pollutant breakdown. Leveraging the power of experimental design methodologies, specifically Response Surface Methodology (RSM), we endeavour to optimize the operational variables governing the photocatalytic degradation of MO using Fe nanoparticles, paving the way for sustainable and efficient wastewater treatment solutions.

EXPERIMENTAL

Chemicals Used

The iron precursor, FeCl2 (99.98%), sourced from Genuine Chemicals in Vellore, India, was utilized in this study. To mitigate photochemical reactions, the required solutions were freshly prepared using double distilled water and stored in light-protected conditions. Prior to usage, all glassware underwent thorough cleaning in a new and fresh solution of HNO_3/HCl (3:1 V/V), followed by extensive rinsing with double distilled water and subsequent drying.

Preparation of aqueous stem extracts of *Cissus quadrangularis*

Fresh, healthy *Cissus quadrangularis* stems were obtained from markets in and around Arni and Vellore District. *Cissus quadrangularis* stems that were fresh, healthy, and mature were employed for

this study. Stems were thoroughly cleaned with running tap water to eliminate any dirt or debris on the surface before being rinsed in deionized water and left to dry in the shade at room temperature. The powder was obtained by grinding the dried stem of *Cissus quadrangularis*.15 grams of *Cissus quadrangularis* powder were combined with 250ml of distilled water in a 500ml conical flask and placed in an 80℃ water bath for one hour. The extract was cooled before being filtered using Whatman filter paper and kept in a cold, dry place for future use.[11]

Phytochemical analyses of aqueous stem extract of *Cissus quadrangularis*

Phytochemical analysis was conducted for the aqueous extract of *Cissus quadrangularis* to ascertain the presence of various photo components, including alkaloids, carbohydrates, starch, reducing sugars, proteins, amino acids, tannins, etc.[12]

Biosynthesis of Fe Nanoparticle using aqueous stem extract of *Cissus quandrigularis*

The biosynthesis of iron (Fe) nanoparticles was achieved through the utilization of the aqueous stem extract of *Cissus quadrangularis*. An equal volume of stem extract (1%) and 0.1 M $FeCl_2$ solution was mixed and the mixture was kept in a water bath until a color shift was noted (Yellow – Intense black).[13,14] The mixture containing Fe-NPs was separated and concentrated centrifugation at 10,000 rpm for 15 mins and repeated washing. After, the final solution was cured the resulting Fe- NPs were used in research experiments.[15]

Characterization of the biogenically synthesized Fe NPs from aqueous stem extracts of *Cissus quadrangularis*

UV-VIS Spectral Analysis

After dilution 20 times, aliquots (1 ml) of seaweed extract were periodically sampled and analyzed in the UV-VIS spectrum to track the bio-reduction of ions in the solution. The Shimadzu 1601 spectrometer, which had a resolution of 1 mm and covered the 250–700 nm range, was used to track the sample as a function of reaction time. The reference point utilized was double-distilled water.[16]

Fourier Transform Infra-Red Spectroscopy (FTIR)

The characterization of functional groups at the surface of Fe nanoparticles from aqueous stem extract of *Cissus quadrangularis* was investigated by FTIR analysis. Following total reduction, the reaction mixture was centrifuged three times at 15,000 rpm for 20 minutes to concentrate the iron nanoparticles and exclude any free biomass residue or anything that is not the capping ligand of the nanoparticles.[17] Distilled water was used in place of the supernatant each time. To get dry powder, the filtered suspension was freeze-dried. Lastly, the ALPHA FT-TR spectrometer (from Bruker, Germany) was used to evaluate the dried nanoparticles to identify various functional groups by displaying peaks in the 400–4000 cm^{-1} range.

X-Ray Diffraction (XRD) Analysis

The resultant pellet was re-dispersed in deionized water after the reduced solution was centrifuged for 40 minutes at 8000 rpm. This centrifugation process was repeated three to five times to remove any materials that had adsorbed on the surface of the produced nanoparticles.[17] Fe nanoparticles that had been purified and dried were then analyzed using X-ray diffraction (XRD).

Scanning Electron Microscopy (SEM) with EDAX analysis

Scanning Electron Microscopy (SEM) observations were carried out using a JEOL JSM 6390 equipment operated at an accelerating voltage of 15 kV to investigate the microstructure and size of the Fe NPs. The nanotract type, Ultra Serial Number, U2475ES, was used to quantify the nanoscale materials' particle sizes. Before the sample was checked for uniform distribution, it was sonicated.[18]

Zeta Potential and Particle Size Determination

The average size and stability of the Nanotrac Wave II, Microtrac Inc., particles were determined by analyzing the Zeta Potential and Dynamic Light Scattering (DLS) of produced Iron nanoparticles. The material was combined with deionized water and filtered through 220 nm filter paper for Zeta potential studies.[18]

Antibacterial studies of biogenically synthesized Fe Nanoparticles

Antibacterial investigations were conducted utilizing Gram-negative bacterial strains, including *E. coli, Proteus sp., and Klebsiella sp.,* alongside the Gram-positive bacterial strain *Bacillus sp.,* procured from DKMC Laboratory. The strains were cultivated in a nutrient-rich broth medium consisting of beef extract, peptone, sodium chloride, and yeast extract, adjusted to a pH of 7.0, and then subjected to incubation at 37ºC. Subsequently, the overnight broth cultures were employed to assess the antibacterial efficacy of Fe nanoparticles. The well-established well diffusion technique was employed to evaluate the antibacterial potential. 0.1 ml of standardized inoculums of each test organism was meticulously inoculated in MHA plates. Ensuring uniform distribution, the inoculum was evenly spread across the MHA plate using a sterile swab, followed by the creation of uniformly sized wells via an 8mm standard cork borer. Within these wells, 100 µl of Fe nanoparticles synthesized from *Cissus quadrangularis* stem extract were introduced, alongside standard antibiotics and ferric chloride solution serving as controls. The inoculated plates were then incubated at 37ºC for a period of 24 hours, after which the zone of inhibition was measured.[19]

Photocatalytic Degradation of the Synthetic Azo Dye using Fe-Nps

The synthetic azo dye Methyl Orange was acquired from a local market, with meticulous attention paid to its quality and purity. To prepare the stock solution, 1 gram of Methyl Orange (MO) was meticulously dissolved in 100ml of distilled water, ensuring precise measurements and optimal concentration. Recognizing the sensitivity of azo dyes to most forms of heat sterilization, the dye solution underwent sterilization through membrane filtration, maintaining its integrity and purity throughout the process. Every substance employed in the synthesis procedure adhered to the strict standards of the highest purity and analytical grade, ensuring the reliability and accuracy of the subsequent experiments.[20]

Photocatalytic Degradation Assay

In the assay for photocatalytic degradation the aqueous solution of the azo dye Methyl Orange (MO) served as the substrate for assessing the efficacy of Fe_2 nanoparticles. The catalytic potential was meticulously investigated by introducing 100mg of Fe nanoparticles into 100ml of the MO aqueous solution, followed by thorough agitation using a Magnetic Stirrer to establish equilibrium between the dye molecules and the nanoparticle surface for duration of 30 minutes.[21,22] Notably, the presence of H_2O_2 was observed to enhance the Phytodegradation of Methyl Orange dye, attributed to its capability to generate additional hydroxyl free radicals, thereby augmenting the degradation process. Furthermore, the experiment underwent rigorous analysis employing a colorimeter, with samples meticulously collected at distinct intervals for a comprehensive examination.[23] Quantification of the degradation efficiency was accomplished through meticulous spectroscopic analysis at a wavelength of 450nm, with the percentage of degradation determined utilizing a precise formula. Specifically, the decolourization efficiency (%) was calculated by evaluating the disparity between the starting or dye concentration (Dye (i)) and the residual dye concentration (Dye (r)), subsequently normalized against the initial dye concentration and expressed as a percentage.[24] This meticulous approach ensured accurate assessment and quantification of the photocatalytic degradation process, providing valuable insights into the efficacy of Fe nanoparticles in the photo degradation of synthetic azo dyes.[25,26]

Experimental Design and optimization by Response Surface Methodology (RSM)

In the pursuit of optimizing a complex, multivariable system, Response Surface Methodology (RSM) emerges as a sophisticated and effective approach. Within the scope of this study, RSM was judiciously employed to attain the optimal decolourization efficiency of Methyl Orange, leveraging the robust capabilities of Design Expert 7.0 software. Specifically, the experimental design encompassed four pivotal independent factors: starting/initial dye concentration, pH level, H_2O_2 concentration, and concentration of anion, each meticulously selected for their critical influence on the process at hand.[27] To comprehensively explore the intricate interplay of these factors, the Central Composite Design (CCD), a widely acknowledged and extensively utilized form of RSM, was strategically employed. This design framework facilitated the systematic evaluation of the individual and collective impacts of the four independent variables, offering valuable insights into their synergistic effects on the decolourization process.[28] Through the meticulous execution of RSM within the confines of CCD, this study aimed to unravel the optimal conditions that would yield maximal

decolourization efficiency, thereby enhancing the efficacy and precision of the experimental outcomes.[29]

RESULTS AND DISCUSSION

Preparation of Plant Extract

The Preparation of Plant extract began with meticulous care, as fresh and robust stems of *Cissus quadrangularis* were meticulously cleansed under running water to eliminate any impurities or debris adhering to their surface. Following this thorough cleansing, a swift rinse in deionized water ensured the purity of the stems, which were then left to air dry in a shaded environment at room temperature, as depicted in Fig.-1 and Fig.-2. Once dried, the stems were finely ground to a powder consistency, yielding 15 grams of *Cissus quadrangularis* stem powder. Subsequently, this powder was carefully mixed with 250 ml of distilled water in a conical flask, resulting in the preparation of the aqueous extract, as illustrated in Fig.-3 and Fig.-4.

Fig.-1: Fresh plant of *C. quadrangularis*

Fig.-2: Dried plant of *C. quadrangularis*

Fig.-3: Powdered form of *C. quadrangularis*

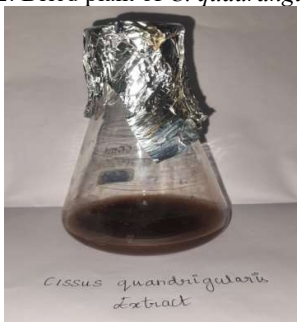

Fig.-4: aqueous extract of *C. quadrangularis*

Phytochemical analysis of *Cissus quandrigularis*

Moving forward, the Phytochemical Analysis of *Cissus quadrangularis* stem extract unfolded, revealing a rich array of phytochemical constituents. These components, including alkaloids, Anthraquinones, flavonoids, saponins, Phytosterols, triterpenoids, and polyphenols, were meticulously scrutinized and their findings documented in Table-1, underscoring the diverse biochemical profile of the plant extract, as depicted in Fig.-5.

Biogenic approach for the biogenesis of Fe Nanoparticles

In the realm of the biogenic method for the production of Iron (Fe) Nanoparticles, the stem extract of *Cissus quadrangularis* played a pivotal role. Illustrated in Fig.-6, the biogenesis of iron nanoparticles initiated a remarkable transformation, as the solution's hue transitioned from colorless to a distinctive mud-red, signaling the presence of the nanoparticles. Subsequent steps involved the separation, concentration, and drying of the solution containing iron nanoparticles. The powdered iron nanoparticle that was the final product was carefully preserved so that it could be used in further experiments, as exemplified in Fig.-6.

Characterization of biogenically synthesized Fe Nanoparticles

UV Analysis

The UV spectroscopic examination revealed distinct absorption peaks characteristic of Fe nanoparticles synthesized from the extract of *Cissus quadrangularis*. The observed absorbance

patterns corroborate the formation of Fe nanoparticles, showcasing their unique electronic transitions and confirming their presence within the synthesized sample. The concoction comprising plant extract and iron chloride was subjected to heating on a hotplate at 100°C, whereupon a discernible transformation ensued. Within 10 minutes, the mixture assumed a brown hue, progressing to a deep, lustrous brown shade after 30 minutes, indicative of the successful synthesis of Fe_2O_3 nanoparticles. The bio-reduction of $FeCl_3$ to produce Fe_2O_3 nanoparticles is responsible for this transition. Subsequent validation of Fe_2O_3 nanoparticle synthesis was accomplished via UV–visible spectroscopy, wherein a prominent absorption peak at 272 nm underscored the presence of synthesized Fe_2O_3 nanoparticles (Fig.-7).

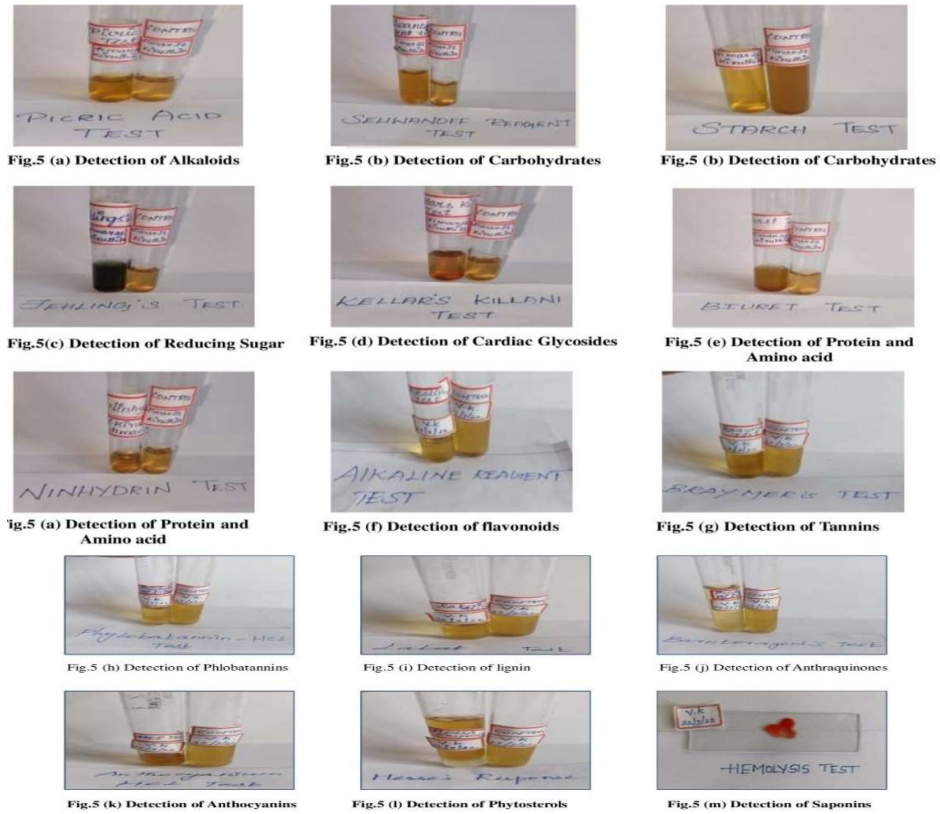

Fig.5 (a) Detection of Alkaloids
Fig.5 (b) Detection of Carbohydrates
Fig.5 (b) Detection of Carbohydrates
Fig.5(c) Detection of Reducing Sugar
Fig.5 (d) Detection of Cardiac Glycosides
Fig.5 (e) Detection of Protein and Amino acid
ig.5 (a) Detection of Protein and Amino acid
Fig.5 (f) Detection of flavonoids
Fig.5 (g) Detection of Tannins
Fig.5 (h) Detection of Phlobatannins
Fig.5 (i) Detection of lignin
Fig.5 (j) Detection of Anthraquinones
Fig.5 (k) Detection of Anthocyanins
Fig.5 (l) Detection of Phytosterols
Fig.5 (m) Detection of Saponins

Fig.-5: Phytochemical Analysis of *C. quadrangularis* Stem Extract

Table-1: Phytochemical Screening of *Cissus quandrigularis* Stem Extract

S. No.	Phyto Constituents	Result
1	Alkaloids	Negative
2	Carbohydrates	Negative
3	Starch	Negative
4	Reducing sugar	Positive
5	Cardiac glycosides	Negative
6	Protein and amino acid	Negative
7	Flavonoids	Negative
8	Tannin	Negative
9	Phlobatannins	Negative
10	Lignin	Negative
11	Anthraquinones	Negative
12	Anthocyanins	Negative
13	Phytosterols	Positive
14	Saponins	Positive
15	Coumarins	Negative

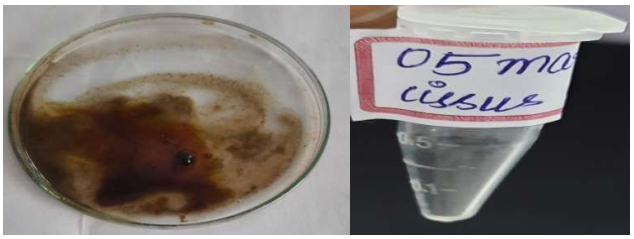

Fig.-6: Biosynthesis of Fe nanoparticles (Wet and Dried Form)

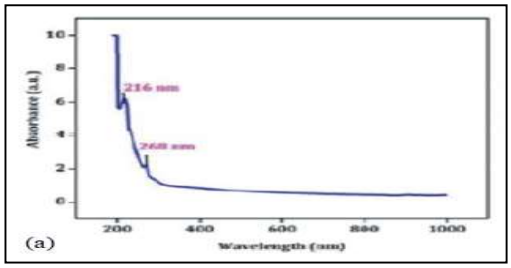

Fig.-7: UV-Vis Absorption Spectra of Fe Nanoparticles

FTIR Analysis

The Fourier-transform infrared spectroscopy (FTIR) analysis unveiled prominent functional groups indicative of the chemical interactions involved in the synthesis process. The spectra demonstrated significant peaks corresponding to specific vibrational modes, elucidating the molecular bonding between the Fe nanoparticles and the phytoconstituents present in the *Cissus quadrangularis* extract, thereby affirming the successful synthesis and functionalization of Fe nanoparticles. The FTIR spectrum delineated distinctive peaks corresponding to both uncalcined and calcined states, manifesting at diverse positions. Within the uncalcined nanoparticles, discernible are two bands positioned at 3321 cm^{-1} and 1,625 cm^{-1}, representing the stretching and blending vibrations of water molecules or hydroxyl groups. This finding indicates that there are still water molecules or certain hydroxide groups on the surface of the nanoparticles as a result of the synthesis taking place in an aquatic environment. In addition, a band attributed to CH_3 deformation developed at 1437 cm^{-1}. On the other hand, the FTIR spectra of the nanoparticles produced by the precipitation approach at 700°C had no lines associated with hydroxyl groups (OH), indicating that all organic species had been completely extracted from the particles after calcination. Following calcination, the spectrum exhibited bands at 537 cm^{-1} and 436 cm^{-1}, attributed to the vibrational signatures of Fe_2O_3 nanoparticles (Fig.-8).

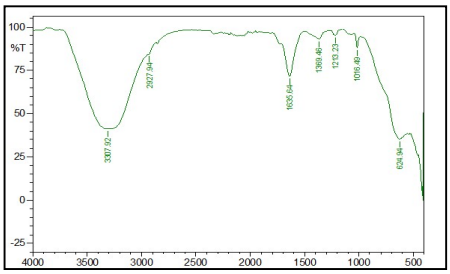

Fig.-8: FTIR analysis of Fe Nanoparticles

XRD Analysis

XRD examination clarified the nature of crystals and phase purity of the synthesized Fe particles. The diffraction patterns exhibited sharp and well-defined peaks, indicative of the crystalline structure of the nanoparticles. Through rigorous analysis and comparison with standard reference data, the crystalline phases and lattice parameters of the Fe nanoparticles were precisely determined, thus providing crucial insights into their structural properties. Moreover, the outcomes of the XRD analysis revealed well-defined peaks at varied angles. These angular measurements unequivocally attest to the crystalline structure of the material under scrutiny. Consequently, it was ascertained that the iron nanoparticles synthesized exhibited a crystalline morphology. Additionally, XRD analysis

corroborated the Nano particulate nature of the biogenesis material, with a typical diameter of 136.43 nm (Fig.-9).

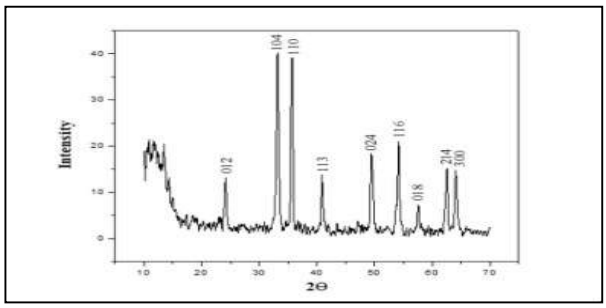

Fig.-9: XRD Analysis of Fe Nanoparticles

SEM-EDAX Analysis

Scanning Electron Microscopy (SEM) (Fig.-10) imaging unveiled the morphological characteristics and surface topography of the synthesized Fe nanoparticles. The micrographs revealed uniform dispersion of nanoparticles with well-defined shapes and sizes, corroborating the effectiveness of the synthesis process. Additionally, high-resolution imaging unveiled intricate surface features and interparticle interactions, shedding light on the nanostructure attributes and confirming the successful fabrication of Fe nanoparticles with desired morphological properties. The obtained nanoparticles are in size from 21 to 82 nm. The altered concentration of reactant of iron chloride and stem extract resulted in unevenly shaped particles on the nanoparticles' surface. It was discovered that the majority of the artificially created Fe_2O_3 NPs were rod- and circular-shaped. A high-intensity peak in the EDX (Fig.-11) elemental diffraction analysis verified the composition of the material. Iron was detected by the first EDX intensity peak, while oxygen was detected by the second intensity peak, which supports the creation of Fe_2O_3 nanoparticles. In addition, a broad peak of chlorine intensity was discovered, which was caused by the chloride in the iron chloride solution. The EDX peak analysis indicates that iron makes up around 57% of the weight, oxygen makes up 35.93 %, and chlorine makes up 8.09%. Furthermore, no further peaks that would have suggested that pure iron oxide nanoparticle production were seen.

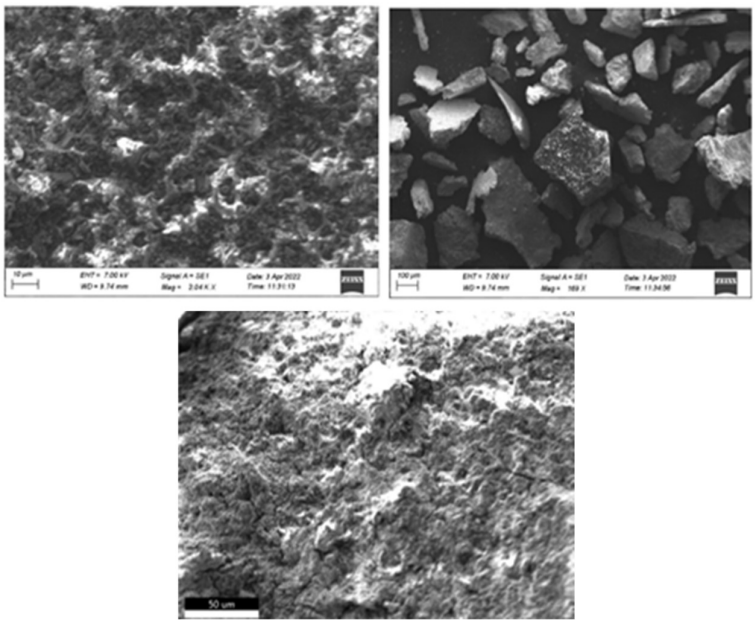

Fig.-10: SEM Analyses of Fe Nanoparticles

Zeta Potential and Measuring of Particle Size

In addition, the stability of the iron nanoparticles was examined using zeta potential and a particle size analyzer. The average size of the iron nanoparticles that were formed was 135.2 nm (Fig.-12), however, the synthesized iron nanoparticles were highly stable with a negative value, or −10.6 mV (Fig.-12).

Antibacterial Activity of Biogenic Fe Nanoparticles

The results suggest that the biogenic Fe nanoparticles synthesized from the stem extract of *Cissus quandrigularis* have significant antibacterial activity against a range of bacterial strains. In comparison to the aqueous plant extract, standard antibiotics (a positive control), and Fe solution (a negative control), the biogenic Fe nanoparticles demonstrated the most pronounced antagonistic effect.

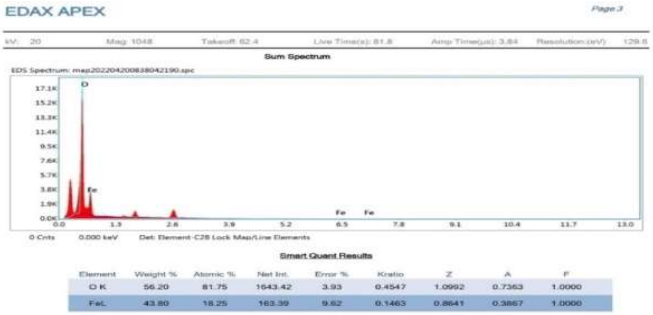

Fig.-11: EDAX and Electron View of Fe Nanoparticle

Specifically, the biogenic Fe nanoparticles showed substantial activity against various bacterial strains, including *E. coli* (25mm), *Staphylococcus sp*. (20mm), *Pseudomonas sp.* (20mm), and *Klebsiella sp.*(20mm), with inhibition zone diameters. This indicates the potential of these nanoparticles as effective antibacterial agents (Fig.-13 and Table-2).

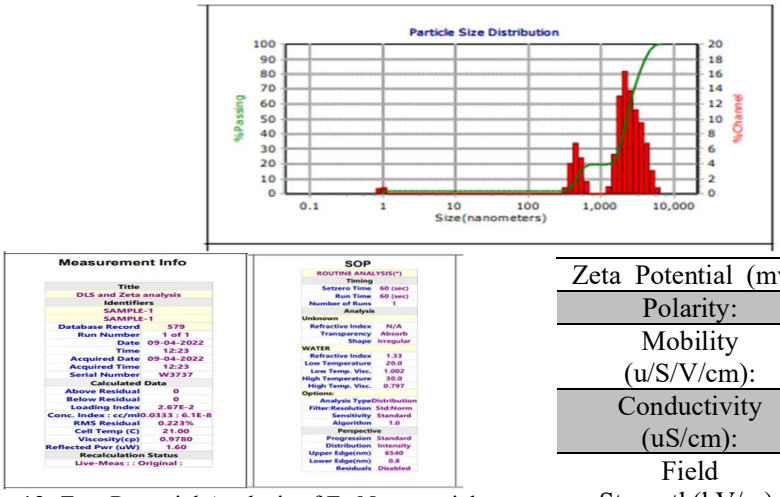

Fig.-12: Zeta Potential Analysis of Fe Nanoparticle

Zeta Potential (mv):	200
Polarity:	Negative
Mobility (u/S/V/cm):	15.63
Conductivity (uS/cm):	622
Field Strength(kV/m):	4.7

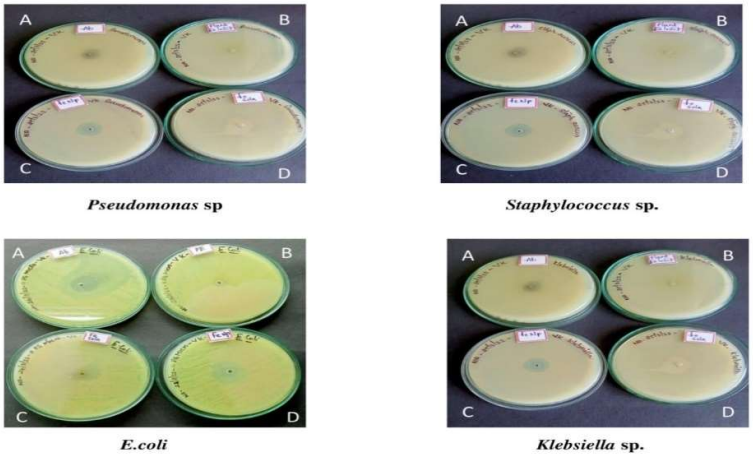

Fig.-13: Antibacterial Activity of Biogenic Fe Nanoparticles from *Cissus quandrigularis*
A. Positive Control; B. Plant Extract; C. Fe NPs; D. Negative Control

Table-2: Antibacterial Activity of Fe Nanoparticles

Bacterial Strains Tested	Fe NPs	Plant extract	Antibiotic	$FeCl_2$ Solution
	Zone of inhibition (mm)			
E.coli	25 mm	3 mm	10 mm	Nil
Klebsiella sp.	20 mm	2mm	10 mm	Nil
Pseudomonas sp.	20 mm	2 mm	10 mm	Nil
Staphylococcus sp.	20 mm	Nil	10 mm	Nil

Photocatalytic Degradation Potential of Fe Nanoparticles

The study examined the iron (Fe) nanoparticles' capacity for photocatalytic degradation using Cissus quadrangularis stem extract, with a focus on Methyl Orange (MO) degradation, an Azo dye (Fig.-14). The experimental setup involved suspending the Fe nanoparticles in the MO dye solution, which was then stirred for 30 minutes on a magnetic stirrer to establish adsorption-desorption equilibrium before initiating the photocatalytic degradation studies in a calorimeter. The graphical representation illustrates the evolution of absorbance of the MO dye over time under irradiation with Fe nanoparticles.[30] Notably, a discernible decline in the peak intensity of MO at 450 nm is observed with increasing irradiation time under UV radiations. Our meticulous analysis reveals that 90% degradation of MO was achieved after 80 minutes, as corroborated by calorimetric analysis at 450 nanometres and visual perception of color. Leveraging the Beer-Lambert Law, which dictates that absorbance intensity is directly proportional to the moieties concentration in solution, our findings elucidate a consistent trend: as time progresses, the absorbance of the solution diminishes, concomitantly escalating the percentage of degradation.[31] Interestingly, when MO was meant solely for photolysis (deterioration under calorimeter conditions), no discernible alteration in dye concentration was noted.[32] This underscores the minimal impact of photolysis on MO degradation. Conversely, when the dye was exposed to Fe nanoparticles, a marginal change in MO concentration was detected, attributed to dye adsorption onto the surface of the Fe nanoparticles. However, when the dye treated with Fe nanoparticles was subjected to Photocatalysis in the calorimeter, a notable improvement in dye degradation was noted, substantiating the significant role of Fe nanoparticles in catalyzing the degradation of Methyl Orange.[33] These findings underscore the promising potential of Fe nanoparticles as efficient catalysts that aid in the photocatalytic breakdown of Methyl Orange, thus warranting further exploration and development in environmental remediation applications[34,35](Fig.-15).

Fig.-14 Photocatalytic activity of Fe Nanoparticles

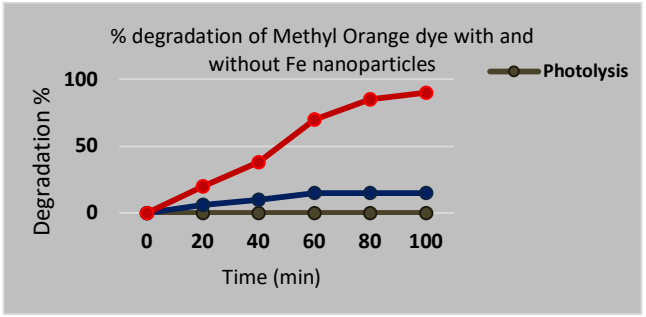

Fig.-15: Photocatalytic Degradation/breakdown of Methyl Orange with and without Fe NPs

Response Surface Methodology for the Design and Optimization of Experiments for the Biodegradation of Methyl Orange

Graphical representations of regression equations offer valuable insights into complex relationships between variables, aiding in the determination of optimal conditions. These three-dimensional

surfaces are pivotal tools for comprehending the intricate interplay among variables within a defined range. The presented figure encapsulates the outcomes of the relationships among four distinct variables and the response, with the objective of optimizing the degradation of Methyl Orange (MO). By graphically depicting these relationships, optimal values can be discerned, facilitating a deeper understanding of variable interactions.

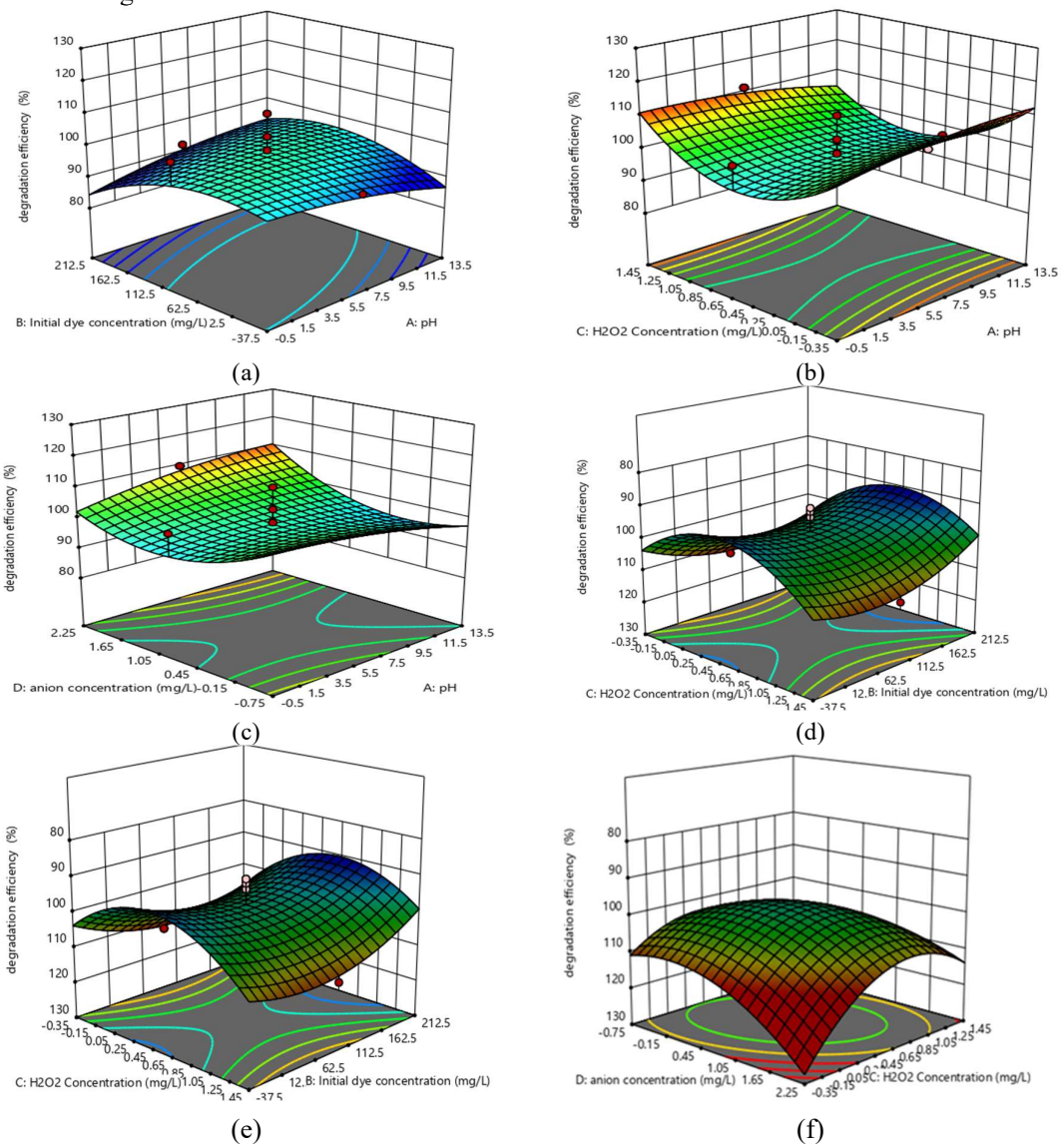

Fig.-16:(a) Illustrates how pH and Initial Dye Concentration Affect MO and Anionic Concentration Degradation Efficiency; (b) Illustrates how pH and H_2O_2 Concentration Affect MO and anionic concentration degradation efficiency;(c) illustrates how H_2O_2 and Anion Concentration Affect MO and pH Degradation Efficiency;(d) illustrates how pH and Anionic Concentration Affect MO Degradation Efficiency; 16(e) illustrates how Anion and Initial Dye Concentration Affect MO Degradation Efficiency; and (f) illustrates the Relationship Between Anion and H_2O_2 concentration and MO Degradation Efficiency

In Fig.-16(a), the MO breakdown efficiency and the concentration of anions are observed to be influenced by pH and initial dye concentration. Insights into the relationship between pH and dye concentration reveal a decrease in degradation efficiency with increasing pH levels, particularly pronounced at higher initial dye concentrations. This phenomenon stems from the surface charge characteristics of the photocatalysts, where an increase in pH leads to heightened repulsion of dye anions due to increased negative charges on the Fe surface. Figure-16(b) illustrates the impact of varying pH levels and H_2O_2 concentrations on MO degradation efficiency and anion concentration. Notably, degradation efficiency improves with increasing H_2O_2 concentration up to a threshold, beyond which it declines gradually. Higher H_2O_2 concentrations facilitate electron-hole recombination

prevention, yet excessive amounts may eliminate essential radicals, diminishing degradation efficiency. Furthermore, Figure-16(c) highlights the gradual decrease in breakdown efficiency as the anion concentration shows a gradual increase. The interplay of pH and anionic species concentration is depicted in Fig.-16(d), indicating a significant influence on MO degradation efficiency.

The impact of initial dye concentration is emphasized in Fig.-16(e), where higher concentrations lead to diminished degradation rates. Conversely, optimal H_2O_2 concentrations (up to 0.53 mg/L) enhance degradation efficiency, aligning with the notion of improved photocatalytic performance. Finally, Figure 16(f) underscores the inverse relationship between dissolved anion concentration and color removal efficiency over time, with higher dye concentrations exacerbating the negative effects of anions through intensified competition for Fe surface adsorption.

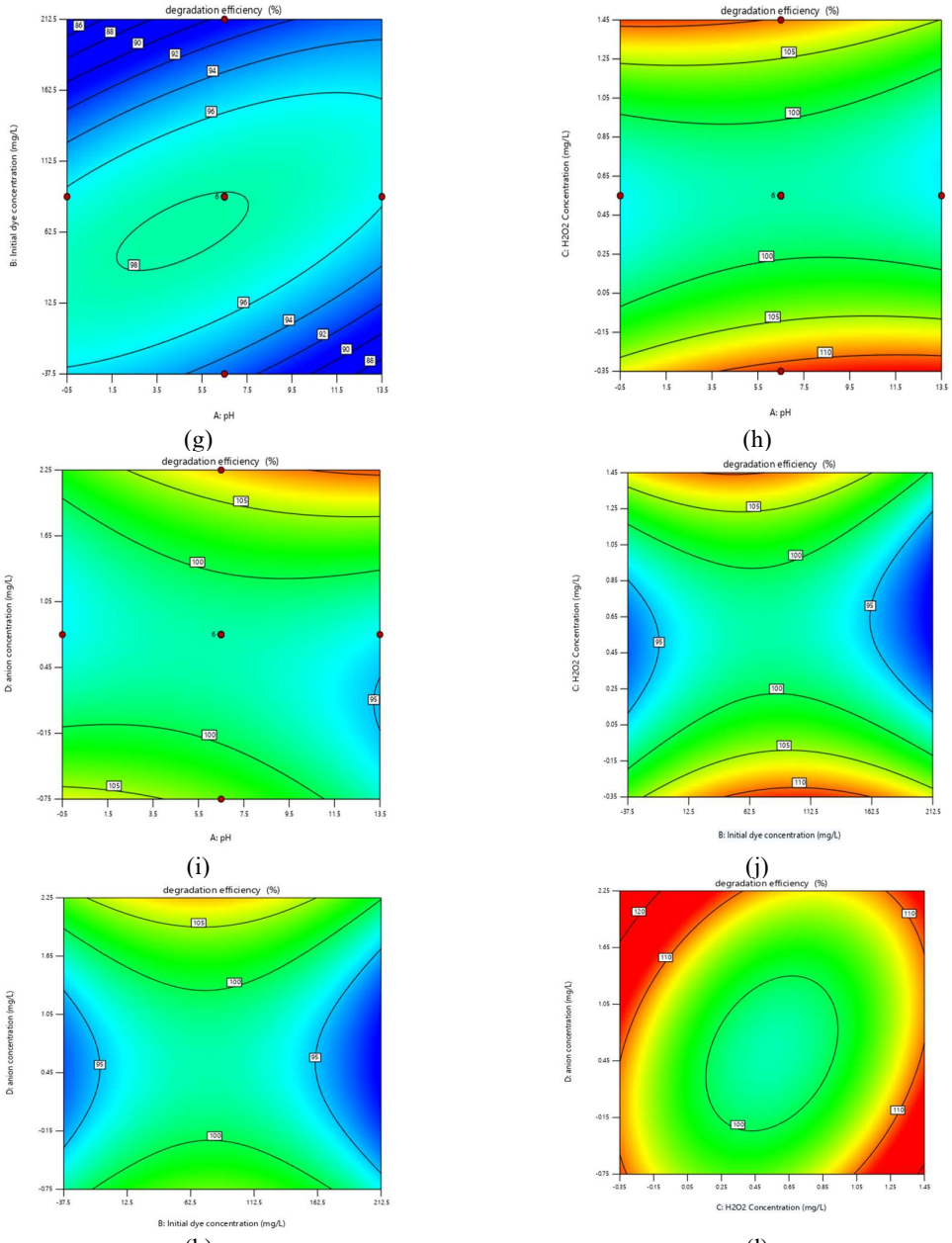

Fig.-16: (g), (h), (i), (j), (k) shows the Counterplots for Hydrogen Ion/pH, starting/Initial Dye Concentration, H_2O_2 Concentration, the Concentration of Anion

These findings collectively elucidate the intricate dynamics governing MO degradation, underscoring the importance of precise control over pH, H_2O_2 concentration, and dye concentration to optimize photocatalytic performance and mitigate environmental pollution.

Table-3: Experimental Range and Independent Test Variables Levels

Variables	Range and Levels	
	-1	+1
pH	3	10
Initial Concentration of Dye (mg/L)	25	150
H2O2 concentration	0.1	1
Anion concentration	0	1.5

CONCLUSION

The biogenic iron (Fe) nanoparticles obtained from *Cissus quadrangularis* stem extract proved to be a rapid process devoid of any toxic or harmful chemicals. Verification of the presence of synthesized Fe nanoparticles was achieved through color change and UV-Vis Spectroscopic analysis, with a notable maximum wavelength at 268nm. FT-IR spectrum analysis further confirmed functional group modifications during the synthesis process. XRD examinations elucidated the typical lattice size of Fe particles from 1.4 to 4.55nm, with a mean particle size distribution of approximately 65nm in aqueous environments. The nanoparticles exhibited a polydisperse particle type with a Zeta Potential value of 200mV, indicating an effective reduction of Fe nanoparticle size by the *Cissus quadrangularis* plant. SEM imaging unveiled the pebble-like structure nanoparticles, with a typical size of less than 50nm and inter-particle spacing also below 50nm. Additionally, EDAX analysis verified the presence of elemental ferric chloride in the Fe nanoparticles. Absorption spectra analysis demonstrated a significant reduction in absorbance with increasing contact time between Iron nanoparticles and Methyl Orange (MO), indicating effective degradation. Photoluminescence spectroscopy further supported MO breakdown under visible light exposure, with a degradation efficiency of 95% after 300 minutes of exposure. The synthesized Fe nanoparticles exhibited high photo-degradation efficiency, reducing MO by 83% and 95% under sunlight and fluorescent light, respectively. Utilizing Response Surface Methodology (RSM), the efficiency of the photocatalytic degradation of Methyl Orange employing Iron nanoparticles was enhanced. Quadratic equations representing the relationship between MO breakdown efficiency and 4 parameters - Hydrogen ion (pH) level, Starting/initial dye concentration, H_2O_2 concentration, and concentration of anion - revealed optimal conditions yielding a degradation efficiency of about 92.24%. These conditions include a starting/initial dye concentration of 25mg/L, 0.52 mg/L of H_2O_2, a Hydrogen ion/pH level of 3, and an anion concentration of 0.69mg/L. In conclusion, the biogenic synthesis of Iron (Fe) nanoparticles from *Cissus quadrangularis* stem extract offers a promising avenue for eco-friendly production of stable nanoparticles with high efficiency in photocatalytic degradation processes, holding significant potential for environmental remediation applications.

ACKNOWLEDGEMENTS

The authors would like to express thanks to PG and Research Department of Microbiology, DKM College for Women (Autonomous),Vellore-632 001.

CONFLICT OF INTERESTS

The authors declare that there is no conflict of interest.

AUTHOR CONTRIBUTIONS

All the authors contributed significantly to this manuscript, participated in reviewing/editing, and approved the final draft for publication. The research profile of the authors can be verified from their ORCID IDs, given below:

Hemapriya Janarthanam https://orcid.org/0000-0001-7216-001X
Reshma Girirajan https://orcid.org/0000-0002-2385-790X
Rajalakshmi Balaji https://orcid.org/my-orcid?orcid=0000-0003-2150-1333
Vijayanand Selvaraj https://orcid.org/0000-0003-1613-9528

REFERENCES

1. S. U. Jadhav, S. D. Kalme, and S. P. Govindwar, *International Biodeterioration and Biodegradation*, **62(2)**,135(2008), https://doi.org/10.1016/j.ibiod.2007.12.010
2. B. Shahmoradi, A. Maleki, K. Byrappa, *Catalysis Science and Technology*, **1**,1216(2011).
3. X. Qu, P.J.J. Alvarez, Q. Li, *Water Research*, **47(12)**, 3931(2013).
4. M.F. Elahmadi, N. Bensalah, A. Gadri, *Journal of Hazardous Materials*,**168**,1163(2009), http://dx.doi.org/10.1016/j.jhazmat.2009.02.139
5. U.G. Akpan, B.H. Hameed, *Journal of Hazardous Materials,* **170**, 520(2009), http://dx.doi.org/10.1016/j.jhazmat.2009.05.039
6. N. John, N.J. Tharayil, M. Somaraj, *Journal* of *Materials Science*: *Materials* in *Electronics*, **28**, 5860(2017), https://doi.org/10.1007/s10854-016-6258- 7
7. R. G. Saratale, G. D. Saratale, D. C. Kalyani, J. S. Chang, and S. P. Govindwar, *Bioresource Technology*, **100(9)**, 2493(2009), https://doi.org/10.1016/j.biortech.2008.12.013
8. J. Jeevanandam, A. Barhoum, Y. S. Chan, and A. Dufresne, *Beilstein Journal of Nanotechnology*, **11(1)**, 179(2018), https://doi.org/10.3762/bjnano.9.98
9. D. Sharma, N. Tiwari, and S. Panwar, *Journal of Nanoscience and Nanotechnology*, **21(8)**, 4872(2021), https://doi.org/10.1166/jnn.2021.19554
10. S. Kanimozhi, R. Durga, M. Sabithasree, A. V. Kumar, A. Sofiavizhimalar, A. A. Kadam, R. Rajagopal, R. Sathya, and N. I. W. Azelee, *Journal of King Saud University*, **34(4)**, 101930(2022), https://doi.org/10.1016/j.jksus.2022.101930
11. J. Saien and Z. Mesgari, *Applied Organometallic Chemistry*, 31(11),1(2017), https://doi.org/10.1002/aoc.3755
12. M, P. R., and P, P. M. Pelagia, *Research Library Advances in Applied Science Research*, **7(4)**, 11(2016), www.pelagiaresearchlibrary.com
13. D. Mukul Pattanayak, P. N. Mohapatra, *Middle East Journal of Scientific Research*, **18(5)**, 623(2013).
14. J. Sivakama Valli, B. Vaseeharan, *Materials Letters*, **82**,171(2012), https://doi.org/10.1016/j.matlet.2012.05.040
15. Sankareswari Anandam, K. Indira, *Applied Biochemistry and Biotechnology*, https://doi.org/10.21203/rs.3.rs-688128/v1
16. N. S. O. Madubuonu, Aisida, I. Ahmad, S. Botha, T. K. Zhao, M. Maaza, (2020), *Applied Physics A Material Science and Processing*, **126(1)**, 72(2020), https://doi.org/10.1007/s00339-019-3249-6
17. S. Parveen, A. H. Wani, M. A. Shah, H. S. Devi, M. Y. Bhat, and J. A. Koka, Microbial. Pathogen, **115**, 287(2018), https://doi.org/10.1016/j.micpath.2017.12.068
18. P. Rajiv, B. Bavadharani, M. N. Kumar, and P. Vanathi, *Biocatalysis and Agricultural Biotechnology*, **12**, 45(2017), https://doi.org/10.1016/j.bcab.2017.08.015
19. N. S. Seddighi, S. Salari, and A. R. Izadi, *IET Nanobiotechnology,* **11**, 883(2017), https://doi.org/10.1049/iet-nbt.2017.0025
20. Pulicherla Yugandar, Thirumalanandhuni Vasavi, Yaganai Jayavardhanrao, *U. M. P. Journal of Cluster Scienec*, **29 (4)**, 743(2018),
21. N. S. Seddighi, S. Salari, and A. R. Izadi, *IET Nanobiotechnology,* **11**, 883(2017), https://doi.org/10.1049/iet-nbt.2017.0025
22. I. Bibi, N. Nazar, S. Ata, M. Sultan, A. Ali, A. Abbas, K. Jilani, S. Kamal, F. M. Sarim, M. I. Khan, F. Jalal, and M. Iqbal, *Journal of Materials Research and Technology*, **8(6)**, 6115(2019), https://doi.org/10.1016/j.jmrt.2019.10.006
23. R. K. Shah, *Arabian Journal of Chemistry*, **16(2)**, 104444(2023), https://doi.org/10.1016/j.arabjc.2022.104444
24. J. Hemapriya, R. Kannan, S. Vijayanand, *Journal of Pure and Applied Microbiology*, **4(1)**, 309(2010),
25. J. Hemapriya, R. Kannan, S. Vijayanand, *Journal of Pure and Applied Microbiology*, **4(1)**, 309(2010)
26. Souhaila Meneceur, Hadia Hemmami, Abderrhmane Bouafia, Salah Eddine Laouini, Mohammed Laid Tedjani, Berra, Djamila and Mahboub, Mohammed Sadok, *Biomass Conversion and Biorefinery*,**14**, 5357(2022), https://doi.org/10.1007/s13399-022-02734-4

27. C. Song, X. Li, L. Wang, and W. Shi, *Scientific Reports*, **6**, 37466(2016), https://doi.org/10.1038/srep37466
28. S. S. A. T. Reza Mahdavi, *Materials Chemistry and Physics*, **267**, 124581(2021), https://doi.org/https://doi.org/10.1016/j.matchemphys.2021.124581
29. A. Z. M. Mohammad Vaez, and S. Alijani, *Industrial and Engineering Chemistry Research*, **51(11)**, 4199(2012).
30. M. S. Hossainand, *Journal of Bangladesh Agricultural University,* **12(1)**, 153(2014)
31. K. Djehaf, A. Z. Bouyakoub Z, R. Ouhib, H. Benmansour, M. A. Bentouaf, *Chemistry International,* **3**,314(2017)
32. M. Iqbal, M. Abbas, J. Nisar,A. Nazir, *Chemistry International*, **5**, 1(2019), https://doi.org/10.5281/zenodo.1475399
33. G. N. Iwuoha, A. Akinseye, *Chemistry International,***5(3)**, 198(2019)
34. M. Laissaoui, Y.Elbatal, I. M. G. Vioque, *Chemistry International*, **3**,343(2017).
35. Abdulrafiu Olaiwola Majolagbe, Adebola Oketola, Oladele Osibanjo, *Chemistry International*, **3**, 58(2017)

[RJC- 8765/2023]